A Platinum Open Access Journal for Organic Chemistry

Paper

Free to Authors and Readers | DOAJ Seal | *Arkivoc* **2023** (ii) 202312038

Selective hydrogen generation from formic acid catalyzed by an iridium-azocarboxamide complex under neat conditions

Mohammad Misbahur Rahman[a], Indranil Dutta[a], Priyanka Chakraborty[a], Nasser A. Alobaid[a], Sandeep Suryabhan Gholap[a], Yadagiri Rachuri[a] , Lujain Alrais,[a] and Kuo-Wei Huang[a, b]*

[a]*KAUST Catalysis Center and Division of Physical Science and Engineering, King Abdullah University of Science and Technology, Thuwal 23955-6900, Saudi Arabia*
[b]*Agency for Science, Technology, and Research, Institute of Materials Research and Engineering and Institute of Sustainability for Chemicals, Energy, and Environment, Singapore 138634, Singapore*
E-mail: hkw@kaust.edu.sa

This work is dedicated to Professor Tien-Yau Luh

Received 06-20-2023 **Accepted Manuscript** 11-17-2023 **Published on line** 12-04-2023

Abstract

A wide range of desirable properties has made formic acid (FA) a favored liquid organic hydrogen carrier in recent years. The state-of-the-art homogenous catalysts generally require a base as an additive in a certain solvent to promote FA dehydrogenation. However, it is crucially important to carry out the reaction without the use of a solvent or any volatile additive in order to achieve optimal efficiency in the process. Herein, we report a series of iridium compounds having an azocarboxamide ligand backbone capable of decomposing FA exclusively into H_2 and CO_2 without the need to use solvents or volatile additives. Under the optimized reaction conditions, a maximum TOF of 12,500 h^{-1} was achieved with no formation of CO.

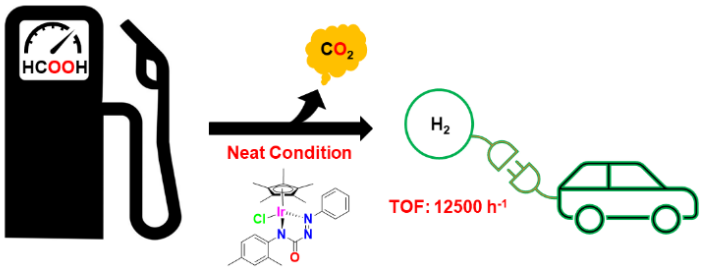

Keywords: Iridium azocarboxamide complex, formic acid dehydrogenation, hydrogen carrier, neat condition.

Introduction

The development of society is correlated with the consumption and utilization of energy. Primary energy consumption has grown from 10037 Mtoe in 2000 to 14314 Mtoe in 2018.[1, 2] Approximately 80% of the world's energy consumption has been fueled by fossil fuels including natural gas, oil, and coal,[1-3] leading to the emission of carbon dioxide (CO_2), which is positively correlated to the substantial rise in the average global atmospheric CO_2 concentrations from 280 ppm in the preindustrial times to ~420 ppm in 2022.[4,5] The capacity of the natural sink (forest, soil, and ocean) to store and remove CO_2 from the atmosphere was limited.[6] The resulting anthropogenic greenhouse effect is believed to be responsible for climate change, increase in global temperature, ocean acidification, sea level rise, etc,[6] and meeting the goal of maintaining global temperature increase below 1.5°C by 2050 is challenging.[6, 7] Out of all sectors, the transportation sector is heavily reliant on fossil fuels, accounting for approx. a quarter of overall CO_2 emissions in 2021.[8] CO_2 emission in the transportation sector has bounced back from 7.1 Gt in 2021 to 7.7 Gt in 2022 after the pandemic restrictions were relaxed and vehicle movements began corresponding to their unprecedented drop in 2020.[9] Thus, to mitigate the environmental issues and climate change, and to address the concern posed by the depletion of fossil fuels the development of clean, sustainable and renewable or low-carbon energy technology is urgently needed.[10, 11]

The most well-known choices for these technologies include renewable biofuels, nuclear power, solar, wind, and hydroelectric energy. Nonetheless, the intermittency of renewable energy suggests that energy carriers are needed for the transportation sector to be electrified to reduce its carbon footprint.[12] However, the electrification of the transportation sector faces significant challenges due to the low volumetric and gravimetric energy densities of batteries, as well as their relatively short lifespan, which could lead to costly replacement and recycling procedures.[13] In this regard, hydrogen (H_2) is considered as a potential substitute that provides intermediate energy storage between power generation plants and end-user applications.[14-18] In 2019, International Energy Agency predicted that H_2 may play a crucial role in a clean, secure, and affordable energy future.[19] According to the 1.5°C roadmap proposed by the International Renewable Energy Agency (IRENA), electrification and efficiency are the main transitional forces facilitated by renewable energy, clean hydrogen, and sustainable biomass.[3] The gravimetric energy density of H_2 is high (33.3 kW·h/kg) and can be efficiently turned into power by the fuel cells with water being produced as the byproduct in the process.[20] However, due to hydrogen's low volumetric energy capacity, there is a significant energy loss during compression and liquefaction, and its storage time is short because it boils out during transit.[18] Furthermore, the lack of viable storage and transportation technologies has significantly limited the applications of H_2.[18, 21-23]

Liquid organic hydrogen carriers (LOHCs) can provide an alternate solution by eliminating the step for compression and paving a safer path through chemically bonding hydrogen to a stable organic liquid carrier.[24] LOHCs follow the concept of hydrogenation and dehydrogenation process via reversible chemical reactions.[25, 26] They provide a safer, cost-effective and feasible pathway to transport hydrogen.[26] Formic acid (FA) is the most basic form of carboxylic acid and a versatile chemical and liquid under ambient conditions. FA has drawn a lot of interest as a promising candidate for LOHC as it has a reasonably high H_2 content (4.38 wt %), environmentally benign low toxicity and low flammability under normal circumstances.[1, 12, 27] Its volumetric capacity is high (53g H_2/L), comparable to the volumetric capacity of the commercial compressed H_2 tank at 700 bar, indicating that FA's energy density is appropriate for H_2 equivalent uses.[1, 12, 28]

Various complexes based on transition metals, such as iron[29-31], rhodium[32, 33], ruthenium[34-38] and iridium,[39-41] have been reported as active catalysts for formic acid dehydrogenation. These reactions often require the aid of the FA/NEt_3 azeotrope[42-44], FA/formate[40, 45, 46] mixtures to achieve the enhanced activity. However, the

efficiency of the process may be affected by the use of solvents and other substances that may easily evaporate. In this regard, neat FA dehydrogenation may be advantageous to achieve high H_2 carrying capacity. In recent years, some instances of homogenous catalysts made up of iridium and ruthenium metal complexes have been documented to accomplish neat FA dehydrogenation. Williams and co-workers in 2016 investigated an iridium-based catalyst for neat formic acid dehydrogenation and reported a high TON of 2.16 million.[47] In 2017, the Gelman group studied an amine-functionalized Ir(III)-PC(sp^3)P catalyst that resulted in a TON of 383,000 and a TOF of 11,760 h^{-1} under neat conditions.[48] Fischimeister and co-workers in 2019, also reported IrCp* (dipyridylamine) catalyst for the dehydrogenation of neat formic acid achieving TOF of 13,292 h^{-1} at 100°C.[49] Recently, the Milstein group has achieved a high TON of 1,701,150 for FA dehydrogenation in neat conditions employing a ruthenium 9H-acridine pincer complex.[50] As part of our continuous efforts in designing and developing catalysts for FA dehydrogenation, herein, we report the synthesis and characterization of a set of iridium complexes with an azo backbone. The catalytic aptitude of the title complexes towards FA dehydrogenation under neat conditions was also evaluated.

Results and Discussion

Treatment of *N*-bromosuccimide with hydrazine-carboxamide derivatives (**L1**, **L2**) in the presence of pyridine, afforded the deep red-colored azo-carboxamide ligands (**L3**, **L4**) (Scheme 1). ^{1}H NMR of ligand **L3**, shows all the characteristic spectra along with the absence of N-H proton of **L1** at δ 7.70 ppm and 8.10 ppm. The aromatic protons and singlet of the methyl proton have been shifted downfield as compared to **L1**. A very similar characteristic pattern was observed for **L4** where the disappearance of N-H proton of **L2** at δ 7.99 ppm and 7.79 ppm, confirmed the formation of an azo backbone.

Ligand **L3** was deprotonated in the presence of trimethylamine (NEt_3) and the subsequent addition of $[Cp^*IrCl_2]_2$ afforded a green-colored complex **Ir-1** at room temperature. The compound **Ir-1** showed signals in the ^{1}H NMR that corresponded to the aromatic protons (δ 7.99–7.20 ppm). When compared to the initial precursor, the singlet of the methyl group from the azo-carboxamide ligand L3 and Cp* appeared at δ 2.31 ppm and 1.22 ppm, both showing a similar but somewhat upfield-shifted spectrum. The disappearance of −NH proton at δ 8.43 ppm in **Ir-1** complex indicated the deprotonation and the amide nitrogen coordination to the metal.

A similar procedure was followed to synthesize **Ir-2** complex using **L4** ligand (Scheme 2). The ^{1}H NMR spectrum of the **Ir-2** complex appeared in the aromatic region at δ 7.85−6.91 ppm which was shifted to upfield as compared to the free ligand (**L4**) and the singlet for the two-methyl group of azo-carboxamide ligand was observed at δ 2.27 and 2.28 ppm. The singlet corresponding to the methyl of the Cp* ligand at δ 1.22 ppm was also shifted upfield as compared to the precursor. The absence of N-H proton at δ 8.26 ppm confirmed the *N,N* coordination to the metal center. The complexes **Ir-1** and **Ir-2** were air-stable and were purified and isolated by column chromatography over basic alumina. The green crystal for each complex, **Ir-1** and **Ir-2**, were afforded by a slow diffusion hexane in a dichloromethane solution and were characterized by X-ray crystallography (Figure 1 and Figure 2).

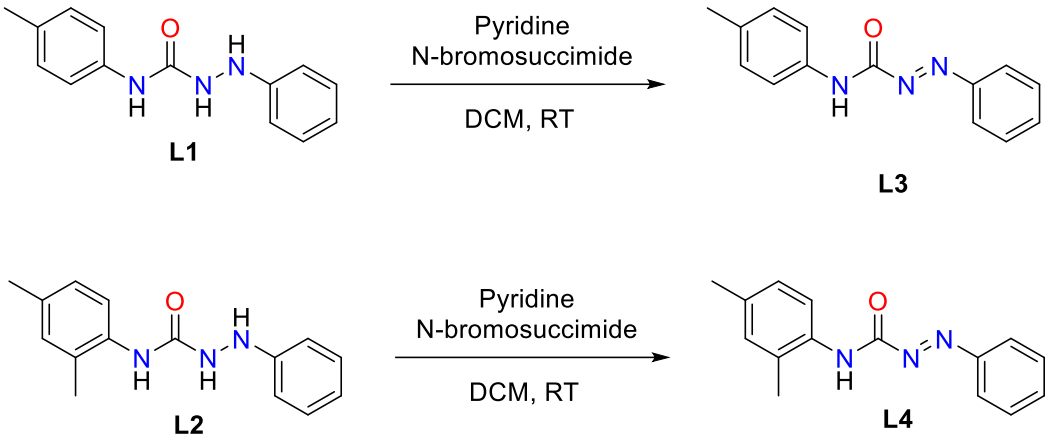

Scheme 1. Synthesis of Ligand, **L3** and **L4.**

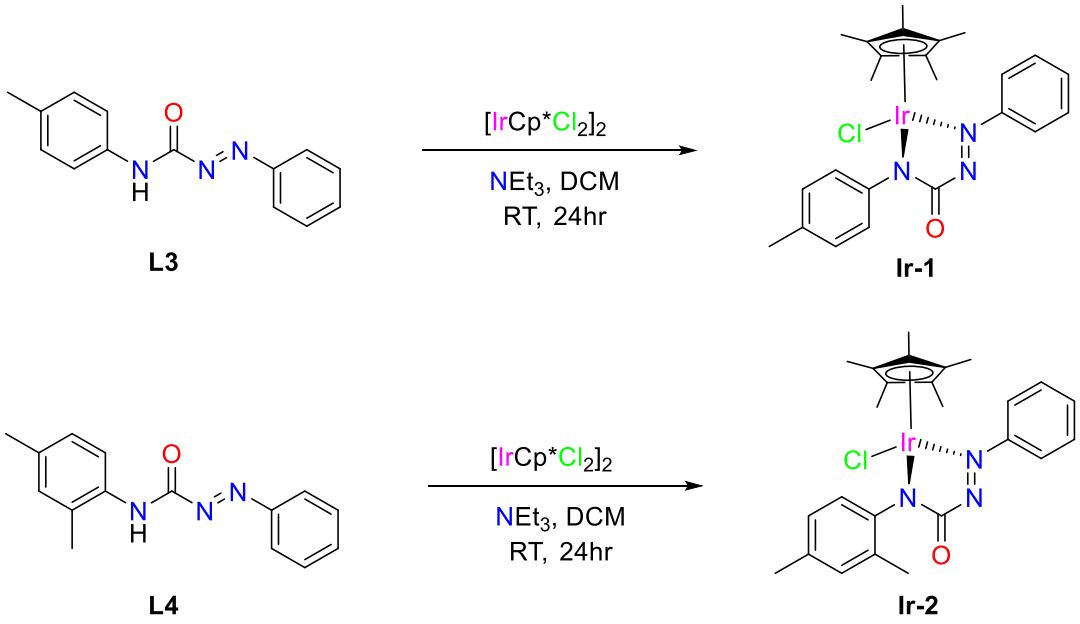

Scheme 2. Synthesis of Iridium complexes, **Ir-1** and **Ir-2.**

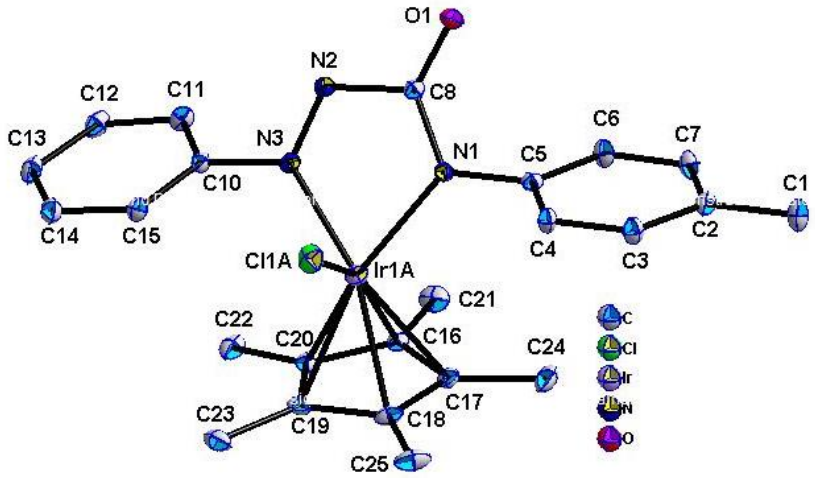

Figure 1. Crystal structure of complex **Ir-1**. Selected Bond lengths(Å) and bond angles(°): Ir1A N1 2.069(3); Ir1A N3 2.029(3); Cl1A Ir1A 2.4079(9); C20 Ir1A 2.190(3); C19 Ir1A 2.185(4); C18 Ir1A 2.199(4); C17 Ir1A 2.205(4); C16 Ir1A 2.153(4); N3 Ir1A N1 73.83(12); N3 Ir1A Cl1A 89.21(9); N1 Ir1A Cl1A 88.16(9).

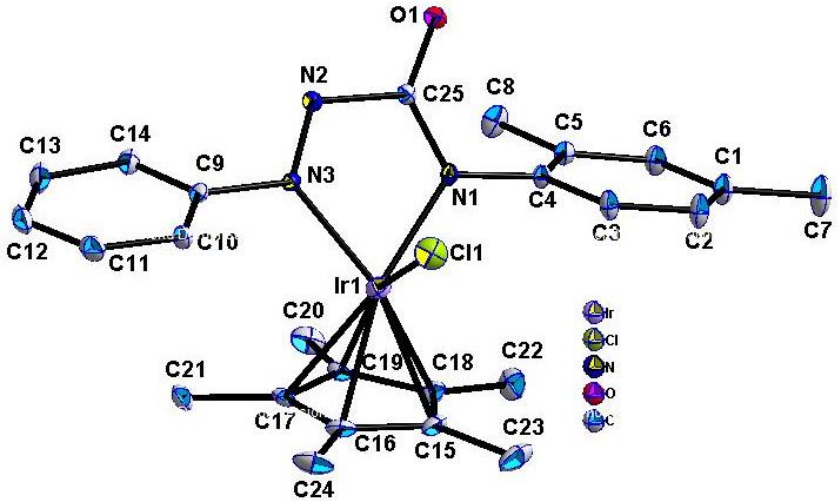

Figure 2. Crystal structure of complex **Ir-2**. Selected Bond lengths(Å) and bond angles(°): Ir1 N1 2.068(2); Ir1 N3 2.023(2); Ir1 C19 2.163(3); Ir1 C15 2.186(3); Ir1 C16 2.192(3); Ir1 C18 2.202(3); Ir1 C17 2.205(3); Ir1 Cl1 2.4055(7); N3 Ir1A N1 73.95(12); N3 Ir1A Cl1 89.30(8); N1 Ir1A Cl1 88.07(9).

The Ir center creates a half-sandwich piano-stool geometry with three legs in both complexes (**Ir-1** and **Ir-2**). The legs of **Ir-1** and **Ir-2** are occupied by N_{azo}, N_{amide}, and Cl, and the seat of the piano-stool is occupied by the Cp* ring. Except for small experimental variances, all complexes exhibit almost similar bond lengths and bond angles. The Cp* ring coordinates with the Ir center in η^5 fashion, where the centroid of the Cp* ring and the Ir centers are separated by 1.812 Å for complex **Ir-1** and 1.816 Å for complex **Ir-2**, respectively (Table 1). The Ir-N_{azo} bond length in **Ir-1** (2.029 Å) is slightly shorter than in **Ir-2** (2.023 Å); however, Ir-N_{amide} bond lengths are very similar. Ir-Cl bond length in **Ir-2** (2.4055 Å) is shorter than **Ir-1** (2.4079 Å) (Table 1).

Table 1. Comparison of selected metric parameters in **Ir-1** and **Ir-2**

Metric parameters	**Ir-1**	**Ir-2**
Ir–Cl	2.4079(9)	2.4055(7)
Ir–N(Azo)	2.029(3)	2.023(2)
Ir–N(Amide)	2.069(3)	2.068(2)
Ir–cp*(centroid)	1.812(2)	1.816(2)
N–N(ligand)	1.266	1.261
N^N chelating angle	73.83	73.94

Formic acid dehydrogenation

We initially conducted the dehydrogenation of formic acid using complex **Ir-1** under neat conditions and in the presence of sodium formate (NaOOCH). 10 µmol of **Ir-1** in the presence of sodium formate with acid-base ratio 2 at 90°C resulted in a TOF of 9700 h^{-1} with incomplete conversion (Table 2, entry1). However, employing 10 µmol of **Ir-2** afforded a TOF of 10600 h^{-1} with 95% conversion (Table 2, entry 2). With a better performing **Ir-2**, further screening with the different ratios of acid-base equivalent at 90°C was studied. A decreased TOF of 9300 h^{-1} was observed on decreasing acid-base ratio to 1 (Table 2, entry 3). Even, by increasing the acid-base ratio to 4, the TOF was decreased to 6000 h^{-1} with an incomplete conversion (Table 2, entry 4). As no gas evolution was observed without base (Table 2, entry 5), which confirmed that it plays a crucial role. A different base, Et_3N resulted in no gas evolution (Table 2, entry 6). FA dehydrogenation dependence on catalyst loading was further screened. The incomplete conversion was observed when the catalyst loading was reduced to 5 µmol (Table 2, entry 7). While on using 15 µmol, both catalysts **Ir-1** and **Ir-2** showed no further improvement (Table 2, entries 8 and 9). The effect on TOF at different reaction temperatures was also studied using complex **Ir-2**. The reactivity of the reaction has significantly decreased with a TOF of 5300 h^{-1} on lowering the temperature to 80°C (Table 2, entry 10) and slightly improved reactivity was observed with a TOF of 12500 h^{-1} on elevating the temperature to 100°C (Table 2, entry 11). Gas volume at different temperatures with respect to time for **Ir-2** (10 µmol) has been depicted in the graph (Figure S1, supporting information).

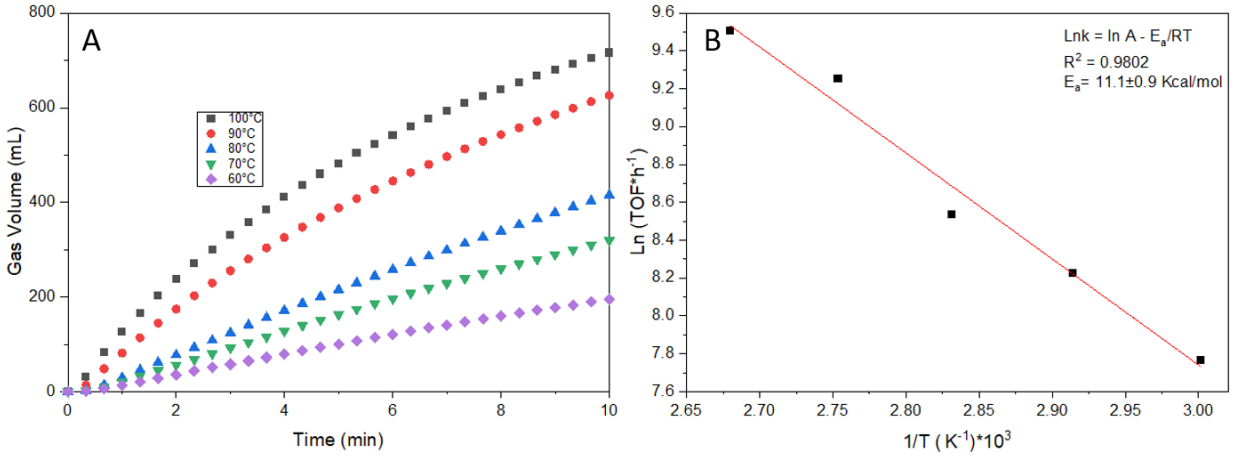

Figure 3. (A) The gas evolution over time to decompose FA at various temperatures. (B) Arrhenius plot for dehydrogenation of FA based on initial TOF values (for first 3 min) using **Ir-2** complex.

Table 2. Ir-carboxamide catalyzed formic acid dehydrogenation[a]

Entry	Cat.	T (°C)	Cat. [μmol]	Acid: Base	H_2+CO_2 [mL]	Conversion [%][b]	TOF [h^{-1}][c]
1	**Ir-1**	90	10	2	265	20	9700
2	**Ir-2**	90	10	2	1230	95	10600
3	**Ir-2**	90	10	1	1240	96	9300
4	**Ir-2**	90	10	4	300	23	6000
5[d]	**Ir-2**	90	10	-	-	-	-
6[e]	**Ir-2**	90	10	2	-	-	-
7	**Ir-2**	90	5	2	710	55	7900
8	**Ir-2**	90	15	2	1270	98	9900
9	**Ir-1**	90	15	2	310	24	9000
10	**Ir-2**	80	10	2	1210	94	5300
11	**Ir-2**	100	10	2	1270	98	12500

[a] General: No reaction occurred in the absence of catalyst. Sodium formate was used as a base, unless specified. A minimum of two times of each reaction were repeated with an error rate of less than 5%. [b] According to the gas produced, conversions were calculated (Details of the calculations in S.I.) [c] Based on the H_2 production during the first 3 minutes, the maximum TOF was predicted. (Details of the calculation in S.I.). [d] Reaction carried out occurred in the absence of base [e] Base: Et_3N, instead of sodium formate was added to the reaction mixture.

The generated gas was subjected to gas chromatography analysis to verify the catalyst's selectivity towards FA dehydrogenation. It revealed that the evolution of H_2 and CO_2 with no discernible CO production, exhibiting the selectivity Ir-azocarboxamibe catalytic system was remarkable, a necessity of any catalyst to be used in practical applications (Figure 4). Additionally, we evaluated the reaction's activation energy (E_a) throughout a temperature range of 60 to 100 °C. The TOFs of the reaction at 60 °C and 70 °C were found to be 2500 h^{-1} and 3400 h^{-1}, respectively (Table S1, supporting information). Gas volume has been depicted in the graph (Figure 3A) at different temperature with respect to time. From the Arrhenius plot of the initial TOF values, the activation energy for the reaction was found to be 11.1 ± 0.9 Kcal/mol (Figure 3B).

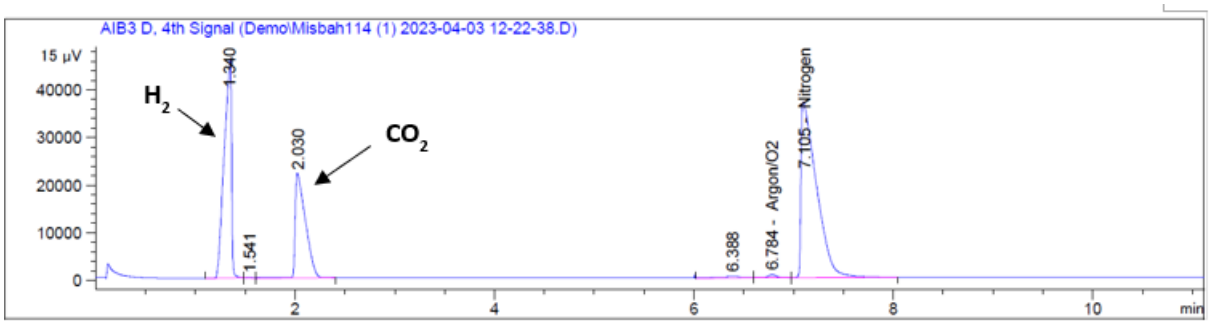

Figure 4. Composition analysis of the generated gas mixture by GC: FA dehydrogenation reaction products (H_2 + CO_2).

Conclusions

To summarize, dehydrogenation of FA is a way to utilize it as a hydrogen carrier. To achieve a functional H_2 economy using FA as a potential hydrogen carrier for storage and transport, it is necessary to minimize the use of solvents and other volatile additives to maximize the efficiency and prevent the poisoning of fuel cells. With this realization of developing a FA dehydrogenation catalyst that performs under neat conditions, herein we have demonstrated a new class of iridium complexes having azocarboxamide ligand backbone. Both complexes were well characterized by spectroscopic techniques. Employing **Ir-2** as a catalyst, a maximum TOF of 12500 h^{-1} was achieved at 100 ºC under solvent-free condition. In both cases, carbon monoxide was not detected in the released gas demonstrating the high selectivity of the system. Further research is needed to fully evaluate the potential and usefulness of the catalyst's latent behavior. Currently, a detailed investigation is ongoing to elucidate the catalytic mechanism.

Experimental Section

General. Commercially available chemicals were used without further purification. If not stated otherwise, all experiments involving metal complexes were conducted in a glovebox with a dry argon environment or using normal Schlenk methods. All other chemicals were purchased and used exactly as they were given. The Ligands **L1**[51], **L2**[51], **Ir-1**[52] and **Ir-2**[52] were synthesized according to literature procedures. On a Bruker 600 MHz spectrometer, the ^{1}H and ^{13}C NMR spectra were recorded. On basic alumina gel (5 wt %), column chromatography was carried out using a DCM/ MeCN gradient (1:0:1:0). For GC analysis, a Techcomp GC7890II with a TCD and FID is used. X-ray diffraction data were collected on a Bruker D8 VENTURE/PHOTON100 CMOS diffractometer at 120 K for the complex **Ir-1** 150 K for the complex **Ir-2**. Mirror-monochromated Mo Kα radiation (λ = 0.71073 Å) source was used for data collection. For data processing, the SAINT[1] packages were used. Multi-scan absorption corrections were made for all the cases using the program SADABS2[1,2]. Structures were solved by direct and Fourier methods and refined by full-matrix least squares based on F^2 using olex-2.[3]

Synthesis of Ligand (L1). Triethylamine (6.3 mmol) was added to the solution of phenylhyadrazine hydrochloride (3mmol) in dichloromethane (5 mL). 4-Methylphenyl isocyanate (3.3 mmol) was dissolved in 5 mL of dichloromethane and was added to the above reaction mixture through the syringe. The mixture was stirred for 2 hours and finally washed with dichloromethane and hexane. The resulting white solid was dried under a vacuum. ^{1}H NMR (500 MHz, DMSO-d_6): δ 8.56 (b, 1H), 8.10 (b, 1H), 7.70 (b, 1H), 7.41-7.39 (d, *J* 8.1Hz, 2H), 7.19-7.16 (t, 2H), 7.03- 7.02 (d, *J* 8.2Hz, 2H), 6.79-6.73 (m, 3H), 2.21 (s, 3H). ^{13}C NMR (500 MHz, DMSO-d_6): δ 156.64, 149.44, 137.16, 130.51, 128.87, 128.77, 118.97, 118.85, 112.53, 20.33

Synthesis of Ligand (L2). Triethylamine (6.3 mmol) was added to the solution of phenylhyadrazine hydrochloride (3 mmol) in dichloromethane (5 mL). 4-Methylphenyl isocyanate (3.3 mmol) was dissolved in 5 mL dichloromethane and was added to the above reaction mixture through the syringe. The mixture was stirred for 2 hours and finally washed with dichloromethane and hexane. The resulting white solid was dried under a vacuum. ^{1}H NMR (500 MHz, DMSO-d_6): *δ* 8.23 (b, 1H), 7.95 (b, 1H), 7.79 (b, 1H), 7.50-7.49 (d, *J* 8.1Hz, 1H), 7.21-7.18 (t, 2H), 6.95-6.92 (t, 2H), 6.82-6.81 (d, *J* 8.0Hz, 2H), 6.78-6.75 (t, 1H), 2.21 (s, 3H), 2.08 (s, 3H). ^{13}C NMR (500 MHz, DMSO-d_6): δ 157.07, 149.37, 134.57, 132.60, 130.85, 129.43, 129.11, 126.77, 122.88, 119.44, 112.65, 20.57, 17.58

Synthesis of Ligand (L3). The Ligand L3 was synthesized using a procedure slightly modified from a reported method.[53] The stirred solution of *N*-(4-Methylphenyl)-2-phenylhydrazinecarboxamide (1 mmol) in dichloromethane (10 mL) was kept at 0°C. Pyridine (1 mmol) was added to this cold solution with stirring. Further, *N*-bromosuccinimide (1.02 mmol) was added over 5–6 min at 0°C. The mixture was further stirred for 1 h and the color of the solution changed to deep red. The solution was washed with brine solution (3×20 mL) and dried over anhydrous sodium sulfate. On evaporating the solvent, deep red color solid was obtained in 92% yield. Experimental mp 104-106 °C. Reported mp 105-107 °C.[53] The desired product was fully characterized by ^{1}H, ^{13}C NMR spectroscopies. ^{1}H NMR (500 MHz, $CDCl_3$): *δ* 8.43 (b, 1H), 8.01-7.99 (d, *J* 8.0Hz, 2H), 7.63-7.59 (m, 3H), 7.56-7.53 (t, 2H), 7.22- 7.20 (d, *J* 8.1Hz, 2H), 2.36 (s, 3H). ^{13}C NMR (400 MHz, $CDCl_3$): *δ* 156.88, 150.85, 134.86, 134.09, 133.90, 129.73, 129.33, 124.13, 119.57, 20.89. ESI-MS (+ve): {[**L3**]+Na^+}; $C_{14}H_{13}N_3ONa$; Calcd. : *m/z* = 262.0951 ; found*: m/z* = 262.0967.

Synthesis of Ligand (L4). The Ligand L4 was synthesized using a procedure slightly modified from a reported method.[53] The stirred solution of *N*-(2,4-dimethylphenyl)-2-phenylhydrazinecarboxamide (1 mmol) in dichloromethane (10 mL) was cooled at 0°C. Pyridine (1 mmol) was added to this cold solution with stirring. Further, *N*-Bromosuccinimide (1.02 mmol) was added over 5–6 min at 0°C. The mixture was further stirred for 1 h and the color of the solution changed to deep red. The solution was washed with brine solution (3×20 mL) and dried over anhydrous sodium sulfate. On evaporating the solvent, deep red color solid was obtained in 92% yield. The desired product was fully characterized by ^{1}H, ^{13}C NMR spectroscopies. ^{1}H NMR (500 MHz, $CDCl_3$): *δ* 8.26 (b, 1H), 8.01-7.99 (d, *J* 8.0Hz, 2H), 7.63-7.59 (m, 3H), 7.56-7.53 (t, 2H), 7.22- 7.20 (d, *J* 8.1Hz, 2H), 1.48 (s, 9H), 2.36 (s, 3H).^{13}C NMR (500 MHz, $CDCl_3$): *δ* 157.33, 150.97, 135.50, 134.10, 132.19, 131.45, 129.53, 128.83, 127.75, 124.37, 121.83, 21.04, 17.65. ESI-MS (+ve): {[**L4]**+Na^+}; $C_{15}H_{15}N_3ONa$; Calcd. : *m/z* = 276.1107 ; found: *m/z* = 276.1117. mp 108-110 °C.

Synthesis of Ir-1. To a stirred solution of Ir precursor $[Cp^*IrCl_2]_2$ (79.7 mg, 0.1 mmol, 1 equiv) in dichloromethane (10 mL), N,2-diphenyldiazenecarboxamide L1 (45.1 mg, 0.2 mmol, 2 equiv) and triethylamine (0.2 mL, 1.4 mmol, 14 equiv) were added and was stirred for 24 h at room temperature. After completion, the solvent was removed under rotavapor and then further purified over alumina with a DCM/MeCN gradient (1/1) and the green product was isolated (45 mg, 0.08 mmol, 40%). mp 230-232 °C.The single crystal was grown up by slow diffusion of hexane into dichloromethane. ^{1}H NMR (500 MHz, $CDCl_3$): *δ* 7.94-7.93 (d, *J* 6.2Hz, 2H), 7.51-7.54 (m, 5H), 7.12-7.11 (d, *J* 8.0Hz, 2H), 2.31 (s, 3H), 1.23 (s, 15H). ^{13}C NMR (400 MHz, $CDCl_3$): *δ* 173.42, 154.48, 143.88, 134.79, 132.80, 129.16, 128.77, 125.61, 124.18, 90.95, 21.26, 8.34. ESI-MS (+ve): {[**Ir-1**]+H^+}; $C_{24}H_{27}ClIrN_3OH$; Calcd.: *m/z* = 602.1537 ; found: *m/z* = 602.1469.

Synthesis of Ir-2. To a stirred solution of Ir precursor $[Cp^*IrCl_2]_2$ (79.7 mg, 0.1 mmol, 1 equiv) in dichloromethane (10 mL), N,2-diphenyldiazenecarboxamide L1 (45.1 mg, 0.2 mmol, 2 equiv) and triethylamine (0.2 mL, 1.4 mmol, 14 equiv) were added and was stirred for 24 h at room temperature. The solvent was removed under rotavapor and then further purified over alumina with a DCM/MeCN gradient (1/1) and the green product was isolated (45 mg, 0.08 mmol, 42%). Mp 237-240 °C.The single crystal was grown up by slow diffusion of hexane into dichloromethane. ^{1}H NMR (500 MHz, $CDCl_3$): *δ* 7.86-7.85 (m, 2H), 7.60-7.58 (d, *J* 5.9Hz, 1H), 7.52-7.50 (m, 3H), 6.99 (s, 1H), 6.92-6.91(d, *J* 5.9Hz, 1H), 2.28 (s, 3H), 2.27 (s, 3H), 1.22 (s, 15H); ^{13}C NMR (400 MHz, $CDCl_3$): *δ* 172.34, 154.56, 142.36, 135.14, 133.88, 132.44, 130.52, 128.75, 127.22, 125.12, 123.74, 91.44, 21.15, 18.86, 8.42. . ESI-MS (+ve): {[**Ir-2**]+H^+}; $C_{25}H_{29}ClIrN_3OH$; Calcd.: *m/z* = 616.1694 ; found: *m/z* = 616.1594.

General procedure for formic acid dehydrogenation. Formic acid dehydrogenation experiments were performed in a two-necked round flask equipped with a reflux condenser and a magnetic stirrer at the required temperature. The measured amount of formic acid was 1 mL (26.5 mmol). Out of this, 300 µL of FA was dissolved with the catalyst to prepare the stock, while the remaining 700 µL was mixed with sodium formate (0.9 g, 13.5

mmol). FA and sodium formate mixture were added to the flask and heated to the desired temperature. Once the temperature attained, the catalyst stock solution in FA was added. The evolution of the generated gas was observed and monitored using an ADM G6691A flowmeter simultaneously. The data was collected in every 2 s to the computer by lab view.

Acknowledgements

We thank King Abdullah University of Science and Technology for financial support. This work is dedicated to Professor Tien-Yau Luh.

Supplementary Material

TOF and TON calculations, tables and additional supporting figures, NMR and XRD data are included in the supplementary material file associated to this manuscript.

References

1. Dutta, I.; Chatterjee, S.; Cheng, H.; Parsapur, R. K.; Liu, Z.; Li, Z.; Ye, E.; Kawanami, H.; Low, J. S. C.; Lai, Z.; Loh, X. J.; Huang, K.-W. *Adv. Energy Mater.* **2022**, *12*, 2103799. https://doi.org/10.1002/aenm.202103799
2. Capuano, L. International Energy Outlook 2018 (IEO2018). *US Energy Information Administration (EIA): Washington, DC, USA* **2018**, *2018*, 21.
3. *IRENA (2023), World Energy Transitions Outlook 2023: 1.5°C Pathway, International Renewable Energy Agency, Abu Dhabi.*; https://mc-cd8320d4-36a1-40ac-83cc-3389-cdn-endpoint.azureedge.net/-/media/Files/IRENA/Agency/Publication/2023/Mar/IRENA_WETO_Preview_2023.pdf?rev=c4c2398e169a4243ad37cf67dc441fa8 (accessed 2023/05/11).
4. Keeling, R. F. K., Charles D. (2017). *Atmospheric Monthly In Situ CO2 Data - Mauna Loa Observatory, Hawaii (Archive 2022-11-02). In Scripps CO2 Program Data. UC San Diego Library Digital Collections*; https://doi.org/10.6075/J08W3BHW (accessed 2023/05/11).
5. *IEA (2023), CO2 Emissions in 2022, IEA, Paris https://www.iea.org/reports/co2-emissions-in-2022, License: CC BY 4.0*; (accessed 2023/05/11).
6. *IPCC, 2022: Climate Change 2022: Mitigation of Climate Change. Contribution of Working Group III to the Sixth Assessment Report of the Intergovernmental Panel on Climate Change. Cambridge University Press, Cambridge, UK and New York, NY, USA.* ; https://www.ipcc.ch/report/ar6/wg3/downloads/report/IPCC_AR6_WGIII_FullReport.pdf (accessed 2023/05/11).
7. Greenwashed catalysis? *Nat. Catal* **2022**, *5* (12), 1071-1072. https://doi.org/10.1038/s41929-022-00905-0
8. *UN Environment Programme, Transport*; https://www.unep.org/explore-topics/energy/what-we-do/transport (accessed 2023/06/19).

9. *IEA (2022), Transport, IEA, Paris https://www.iea.org/reports/transport, License: CC BY 4.0*; (accessed 2023/05/11).
10. Chatterjee, S.; Huang, K.-W. *Nat. Commun.* **2020**, *11*, 3287. https://doi.org/10.1038/s41467-020-17203-7
11. Whitesides, G. M.; Crabtree, G. W. *Science* **2007**, *315* (5813), 796-798. https://doi.org/10.1126/science.1140362
12. Eppinger, J.; Huang, K.-W. *ACS Energy Lett.* **2017**, *2*, 188-195. https://doi.org/10.1021/acsenergylett.6b00574
13. Modisha, P. M.; Ouma, C. N. M.; Garidzirai, R.; Wasserscheid, P.; Bessarabov, D. *Energy Fuels* **2019**, *33*, 2778-2796. https://doi.org/10.1021/acs.energyfuels.9b00296
14. Turner, J. A. *Science* **2004**, *305* (5686), 972-974. https://doi.org/10.1126/science.1103197
15. Lewis, N. S.; Nocera, D. G. *PNAS* **2006**, *103*, 15729-15735. https://doi.org/10.1073/pnas.0603395103
16. Moriarty, P.; Honnery, D. *Int. J. Hydrogen Energy* **2009**, *34*, 31-39. https://doi.org/10.1016/j.ijhydene.2008.10.060
17. Moriarty, P.; Honnery, D. *Int. J. Hydrogen Energy* **2010**, *35*, 12374-12380. https://doi.org/10.1016/j.ijhydene.2010.08.060
18. Armaroli, N.; Balzani, V. *ChemSusChem* **2011**, *4*, 21-36. https://doi.org/10.1002/cssc.201000182
19. *IEA (2019), The Future of Hydrogen, IEA, Paris https://www.iea.org/reports/the-future-of-hydrogen, License: CC BY 4.0;* (accessed 2023/05/11).
20. 20. Sordakis, K.; Tang, C.; Vogt, L. K.; Junge, H.; Dyson, P. J.; Beller, M.; Laurenczy, G. *Chem. Rev.* **2018**, *118*, 372-433. https://doi.org/10.1021/acs.chemrev.7b00182
21. Dawood, F.; Anda, M.; Shafiullah, G. M. *Int. J. Hydrogen Energy* **2020**, *45* (7), 3847-3869. https://doi.org/10.1016/j.ijhydene.2019.12.059
22. Abdalla, A. M.; Hossain, S.; Nisfindy, O. B.; Azad, A. T.; Dawood, M.; Azad, A. K. *Energy Convers. Manage.* **2018**, *165*, 602-627. https://doi.org/10.1016/j.enconman.2018.03.088
23. Felderhoff, M.; Weidenthaler, C.; von Helmolt, R.; Eberle, U. *Phys. Chem. Chem. Phys.* **2007**, *9*, 2643-2653. https://doi.org/10.1039/b701563c
24. Preuster, P.; Papp, C.; Wasserscheid, P. *Acc. Chem. Res.* **2017**, *50*, 74-85. https://doi.org/10.1021/acs.accounts.6b00474
25. Niermann, M.; Drünert, S.; Kaltschmitt, M.; Bonhoff, K. *Energy Environ. Sci.* **2019**, *12*, 290-307. https://doi.org/10.1039/C8EE02700E
26. Aakko-Saksa, P. T.; Cook, C.; Kiviaho, J.; Repo, T. *J. Power Sources* **2018**, *396*, 803-823. https://doi.org/10.1016/j.jpowsour.2018.04.011
27. Chatterjee, S.; Dutta, I.; Huang, K.-W. 8 - Power to formic acid. In *Power to Fuel*, Spazzafumo, G. Ed.; Academic Press, 2021; pp 169-210. https://doi.org/10.1016/B978-0-12-822813-5.00006-0
28. Chatterjee, S.; Dutta, I.; Lum, Y.; Lai, Z.; Huang, K.-W. *Energy Environ. Sci* **2021**, *14*, 1194-1246. https://doi.org/10.1039/D0EE03011B

29. Curley, J. B.; Bernskoetter, W. H.; Hazari, N. *ChemCatChem* **2020**, *12*, 1934-1938. https://doi.org/10.1002/cctc.202000066
30. Bertini, F.; Mellone, I.; Ienco, A.; Peruzzini, M.; Gonsalvi, L. *ACS Catal.* **2015**, *5*, 1254-1265. https://doi.org/10.1021/cs501998t
31. Bielinski, E. A.; Lagaditis, P. O.; Zhang, Y.; Mercado, B. Q.; Würtele, C.; Bernskoetter, W. H.; Hazari, N.; Schneider, S. *J. Am. Chem. Soc.* **2014**, *136*, 10234-10237. https://doi.org/10.1021/ja505241x
32. Fukuzumi, S.; Kobayashi, T.; Suenobu, T. *ChemSusChem* **2008**, *1*, 827-834. https://doi.org/10.1002/cssc.200800147
33. Hermosilla, P.; Urriolabeitia, A.; Iglesias, M.; Polo, V.; Casado, M. A. *Inorg. Chem. Front.* **2022**, *9*, 4538-4547. https://doi.org/10.1039/D2QI01056A
34. Guan, C.; Zhang, D.-D.; Pan, Y.; Iguchi, M.; Ajitha, M. J.; Hu, J.; Li, H.; Yao, C.; Huang, M.-H.; Min, S.; et al. *Inorg. Chem.* **2017**, *56*, 438-445. https://doi.org/10.1021/acs.inorgchem.6b02334
35. Pan, Y.; Pan, C.-L.; Zhang, Y.; Li, H.; Min, S.; Guo, X.; Zheng, B.; Chen, H.; Anders, A.; Lai, Z.; et al. *Chem. Asian J.* **2016**, *11*, 1357-1360. https://doi.org/10.1002/asia.201600169
36. Verron, R.; Puig, E.; Sutra, P.; Igau, A.; Fischmeister, C. *ACS Catal.* **2023**, *13*, 5787-5794. https://doi.org/10.1021/acscatal.3c00476
37. Prichatz, C.; Trincado, M.; Tan, L.; Casas, F.; Kammer, A.; Junge, H.; Beller, M.; Grützmacher, H. *ChemSusChem* **2018**, *11*, 3092-3095. https://doi.org/10.1002/cssc.201801072
38. Yaacoub, L.; Dutta, I.; Werghi, B.; Chen, B. W. J.; Zhang, J.; Hamad, E. A.; Ling Ang, E. P.; Pump, E.; Sedjerari, A. B.; Huang, K.-W.; et al. *ACS Catal.* **2022**, *12*, 14408-14417. https://doi.org/10.1021/acscatal.2c04137
39. Onishi, N.; Kanega, R.; Fujita, E.; Himeda, Y. *Adv. Synth. Catal.* **2019**, *361*, 289-296. (acccessed 2023/05/16). https://doi.org/10.1002/adsc.201801323
40. Kanega, R.; Ertem, M. Z.; Onishi, N.; Szalda, D. J.; Fujita, E.; Himeda, Y. *Organometallics* **2020**, *39*, 1519-1531. https://doi.org/10.1021/acs.organomet.9b00809
41. Wang, Z.; Lu, S.-M.; Li, J.; Wang, J.; Li, C. *Chem. Eur. J.* **2015**, *21*, 12592-12595. (acccessed 2023/05/16). https://doi.org/10.1002/chem.201502086
42. Loges, B.; Boddien, A.; Junge, H.; Beller, M. *Angew. Chem. Int. Ed.* **2008**, *47*, 3962-3965. https://doi.org/10.1002/anie.200705972
43. Zell, T.; Butschke, B.; Ben-David, Y.; Milstein, D. *Chem. Eur. J.* **2013**, *19*, 8068-8072. https://doi.org/10.1002/chem.201301383
44. Dutta, I.; Alobaid, N. A.; Menicucci, F. L.; Chakraborty, P.; Guan, C.; Han, D.; Huang, K.-W. *Int. J. Hydrogen Energy* **2022**. https://doi.org/10.1016/j.ijhydene.2022.04.220
45. Fellay, C.; Dyson, P. J.; Laurenczy, G. *Angew. Chem. Int. Ed.* **2008**, *47*, 3966-3968. https://doi.org/10.1002/anie.200800320
46. Kanega, R.; Onishi, N.; Wang, L.; Murata, K.; Muckerman, J. T.; Fujita, E.; Himeda, Y. *Chem. Eur. J.* **2018**, *24*, 18389-18392. https://doi.org/10.1002/chem.201800428
47. Celaje, J. J. A.; Lu, Z.; Kedzie, E. A.; Terrile, N. J.; Lo, J. N.; Williams, T. J. *Nat. Commun.* **2016**, *7*, 11308.

https://doi.org/10.1038/ncomms11308
48. Cohen, S.; Borin, V.; Schapiro, I.; Musa, S.; De-Botton, S.; Belkova, N. V.; Gelman, D. *ACS Catal.* **2017**, *7*, 8139-8146.
https://doi.org/10.1021/acscatal.7b02482
49. Wang, S.; Huang, H.; Roisnel, T.; Bruneau, C.; Fischmeister, C. *ChemSusChem* **2019**, *12*, 179-184.
https://doi.org/10.1002/cssc.201802275
50. Kar, S.; Rauch, M.; Leitus, G.; Ben-David, Y.; Milstein, D. *Nat. Catal* **2021**, *4*, 193-201.
https://doi.org/10.1038/s41929-021-00575-4
51. Cappoen, D.; Majce, V.; Uythethofken, C.; Urankar, D.; Mathys, V.; Kočevar, M.; Verschaeve, L.; Polanc, S.; Huygen, K.; Košmrlj, J. *Eur. J. Med. Chem.* **2014**, *74*, 85-94.
https://doi.org/10.1016/j.ejmech.2013.12.057
52. Chandra, S.; Kelm, O.; Albold, U.; Hazari, A. S.; Urankar, D.; Košmrlj, J.; Sarkar, B. *Organometallics* **2021**, *40*, 3907-3916.
https://doi.org/10.1021/acs.organomet.1c00468
53. Li, J.-P.; Liu, P.; Wang, Y.-L. *J. Chem. Res.* **2003**, *2003*, 109-110.c
https://doi.org/10.3184/030823403103173138